10498 *Inorg. Chem.* **2009**, *48*, 10498–10506
DOI: 10.1021/ic9007763

Inorganic Chemistry
Article

Structure−Activity Correlations Among Iridium(III) Photosensitizers in a Robust Water-Reducing System

Peter N. Curtin, Leonard L. Tinker, Christine M. Burgess, Eric D. Cline, and Stefan Bernhard*

Department of Chemistry, Princeton University, Princeton New Jersey 08544

Received April 22, 2009

A photocatalytic water-reducing system utilizing a *bis*-cyclometalated bipyridyl iridium(III) photosensitizer (PS) and a platinum or palladium heterogeneous catalyst was used to identify systematic property−activity correlations among a library of structural derivatives of $[Ir(ppy)_2(bpy)]^+$. A heterogeneous Pd catalyst proved to be more durable than its previously reported Pt-based counterpart, allowing for more reliable photosensitizer study. The deliberate steric and electronic variations of the ppy and bpy moieties resulted in a dramatic decrease of the degradation rates observed with selected photosensitizers when compared to the more substitution-labile $[Ir(ppy)_2(bpy)]^+$ parent compound. An improved photosensitizer structure with a Pd catalyst in a nonligating solvent exhibited a 150-fold increase in catalyst turnover numbers compared to the system using $[Ir(ppy)_2(bpy)]^+$ and a Pt catalyst. Furthermore, photocatalytic and photophysical studies at varied temperatures provided information on the rate-limiting step of the photocatalytic process, which is shown to be dependent on both the PS and the Pt or Pd catalytic species.

Introduction

Due to the current need for clean and sustainable sources of chemical fuels, the photolysis of water into dihydrogen and dioxygen has become an important area of active research.[1] One approach in the development of a system capable of splitting water has been through the use of molecular catalysts powered by visible light.[2−4] Due to the complexity inherent in the four-electron redox chemistry required by water-splitting catalysis, a typical approach has been to separate water reduction and water oxidation into two separate scientific problems. Ultimately, investigators intend to integrate the independently developed components of these catalytic half reactions within a complete molecular water-splitting device.

Molecular photocatalytic water-reducing systems were actively researched in the late 1970s and the 1980s[5−11] and have recently come under investigation once again.[12−23] These systems typically utilize a photosensitizer (PS) for light absorption, an electron relay (ER) to create charge separation, and a sacrificial reductant (SR) to serve as an electron source that allows for the catalytic production of hydrogen without concurrent dioxygen evolution. Historically, ruthenium(II) complexes have been the most common PS choice as either a monomeric species such as $[Ru(bpy)_3]^{2+}$ (bpy = 2,2′-bipyridine)[5−10,12] or as a moiety in a supramolecular

*To whom correspondence should be addressed. Phone: 609-258-3879. Fax: 609-258-6746. E-mail: bern@princeton.edu.

(1) Lewis, N. S.; Nocera, D. G. *Proc. Natl. Acad. Sci. U.S.A* **2006**, *103*, 15729–15735.
(2) Meyer, T. J. *Acc. Chem. Res.* **1989**, *22*, 163–170.
(3) Alstrum-Acevedo, J. H.; Brennaman, M. K.; Meyer, T. J. *Inorg. Chem.* **2005**, *44*, 6802–6827.
(4) Esswein, A. J.; Nocera, D. G. *Chem. Rev.* **2007**, *107*, 4022–4047.
(5) Kalyanasundaram, K.; Kiwi, J.; Gratzel, M. *Helv. Chim. Acta* **1978**, *61*, 2720–2730.
(6) Moradpour, A.; Amouyal, E.; Keller, P.; Kagan, H. *Nouv. J. Chim.* **1978**, *2*, 547–549.
(7) Delaive, P. J.; Sullivan, B. P.; Meyer, T. J.; Whitten, D. G. *J. Am. Chem. Soc.* **1979**, *101*, 4007–4008.
(8) Amouyal, E.; Keller, P.; Moradpour, A. *J. Chem. Soc., Chem. Commun.* **1980**, 1019–1020.
(9) Ziessel, R.; Hawecker, J.; Lehn, J. M. *Helv. Chim. Acta* **1986**, *69*, 1065–1084.
(10) Brown, G. M.; Brunschwig, B. S.; Creutz, C.; Endicott, J. F.; Sutin, N. *J. Am. Chem. Soc.* **1979**, *101*, 1298–1300.
(11) Johansen, O.; Mau, A. W. H.; Sasse, W. H. F. *Chem. Phys. Lett.* **1983**, *94*, 107–112.
(12) Goldsmith, J. I.; Hudson, W. R.; Lowry, M. S.; Anderson, T. H.; Bernhard, S. *J. Am. Chem. Soc.* **2005**, *127*, 7502–7510.
(13) Rau, S.; Schafer, B.; Gleich, D.; Anders, E.; Rudolph, M.; Friedrich, M.; Gorls, H.; Henry, W.; Vos, J. G. *Angew. Chem., Int. Ed.* **2006**, *45*, 6215–6218.
(14) Ozawa, H.; Yokoyama, Y.; Haga, M.; Sakai, K. *Dalton Trans.* **2007**, 1197–1206.
(15) Lei, P.; Hedlund, M.; Lomoth, R.; Rensmo, H.; Johansson, O.; Hammarstrom, L. *J. Am. Chem. Soc.* **2008**, *130*, 26–27.
(16) Elvington, M.; Brown, J.; Arachchige, S. M.; Brewer, K. J. *J. Am. Chem. Soc.* **2007**, *129*, 10644–10645.
(17) Esswein, A. J.; Veige, A. S.; Nocera, D. G. *J. Am. Chem. Soc.* **2005**, *127*, 16641–16651.
(18) Du, P. W.; Schneider, J.; Jarosz, P.; Eisenberg, R. *J. Am. Chem. Soc.* **2006**, *128*, 7726–7727.
(19) Du, P. W.; Schneider, J.; Jarosz, P.; Zhang, J.; Brennessel, W. W.; Eisenberg, R. *J. Phys. Chem. B* **2007**, *111*, 6887–6894.
(20) Du, P. W.; Schneider, J.; Fan, L.; Zhao, W.; Patel, U.; Castellano, F. N.; Eisenberg, R. *J. Am. Chem. Soc.* **2008**, *130*, 5056–5058.
(21) Tinker, L. L.; McDaniel, N. D.; Curtin, P. N.; Smith, C. K.; Ireland, M. J.; Bernhard, S. *Chem.—Eur. J.* **2007**, *13*, 8726–8732.
(22) Cline, E. D.; Adamson, S. E.; Bernhard, S. *Inorg. Chem.* **2008**, *47*, 10378–10388.
(23) Probst, B.; Kolano, C.; Hamm, P.; Alberto, R. *Inorg. Chem.* **2009**, *48*, 1836–1843.

Published on Web 07/16/2009

structure that tethers the PS to a redox catalyst.[13−16] In monomeric Ru(II) PS systems, there is evidence that hydrogen production can vary widely through tuning of the photosensitizer's ligand architecture,[12] and recently, iridium(III) PS structures have come under investigation as superior alternatives to Ru(II) PS species. One class of investigated iridium complexes is based on $[Ir(ppy)_2(bpy)]^+$ (ppy = 2-phenylpyridine).[12,21,22,24−26] The heteroleptic ligand architecture of such complexes allows for the independent tuning of the highest occupied molecular orbital and lowest unoccupied molecular orbital, making a wide range of photophysical and electrochemical properties available.[24] $[Ir(ppy)_2(bpy)]^+$ and its derivatives have already demonstrated improved catalytic performance over ruthenium complexes in homogeneous water-reducing systems.[12,22,26]

One of the difficulties involved in PS study is identifying structure−activity trends in these complicated systems. Specifically, ER decomposition can obscure the influence of PS ligand architecture on catalysis, limiting the extent to which the diverse iridium-based catalysts can be reliably compared.[12] Recently, a system that used a $[Ir(ppy)_2(bpy)]^+$ photosensitizer and operated in the absence of an ER was shown to be limited principally by photosensitizer degradation.[21] This system produces hydrogen by the mechanism shown in Figure 1. An excited PS is reductively quenched by the SR to produce a PS^- that subsequently reduces protons to dihydrogen in a dark reaction catalyzed by a colloidal platinum catalyst (Cat). The identification of PS degradation products in this system motivates the targeting of iridium(III) PS structures with enhanced photostability, and the observed correlation between a change in hydrogen evolution rates and the extent of photosensitizer degradation provides a tool for probing catalyst durability.[21]

In the present study, we investigate correlations between PS structure and catalytic performance in an ER-deficient system. A palladium catalyst is selected for use in place of a previously used platinum catalyst. Palladium catalyst activity is sustained over the course of illumination, while the platinum catalyst is shown to undergo greater degradation. The consistent palladium activity facilitates the more direct study of correlations between photosensitizer durability and observed hydrogen evolution. A combinatorial library of 15 iridium(III) complexes (three C^N ligands and five N^N ligands) was synthesized to provide a basis for elucidating trends. Photophysical measurements were taken to evaluate the existence of property−activity correlations. Upon observation of trends in this combinatorial study, two novel iridium(III) complexes were prepared, characterized, and tested as catalysts in a water-reducing system. Of the PS structures investigated, one was capable of over 6 times as many catalytic turnovers as the parent $[Ir(ppy)_2(bpy)]^+$ structure under identical conditions. Additional optimization of the catalytic conditions allowed for up to 2300 PS turnovers, which is over 150 times the number of PS turnovers previously reported for a similar system incorporating $[Ir(ppy)_2(bpy)]^+$ with a platinum catalyst[21] and demonstrates the advantage of parallel screening using a high-throughput photoreactor. The system's palladium catalyst was shown to be colloidal by transmission electron microscopy (TEM) analysis and through a series of mercury poisoning experiments. Furthermore, photophysical studies and hydrogen photoevolution experiments at varied temperature were conducted to obtain information on the rate-limiting step of the catalytic process and gain insight into the reaction mechanism.

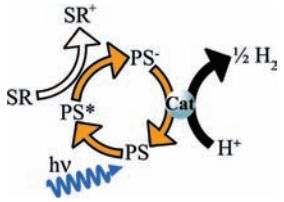

Figure 1. Reductive quenching mechanism for the catalytic production of hydrogen by a $[Ir(ppy)_2(bpy)]^+$ PS in the absence of an electron relay (PS = photosensitizer; SR = sacrificial reductant; Cat = colloidal metal catalyst).

Experimental Procedure

Materials. 2-Phenylpyridine (ppy), 2,2′-bipyridine (bpy), 4,4′-dimethyl-2,2′-bipyridine (4,4′-dmbpy), 5,5′-dimethyl-2,2′-bipyridine (5,5′-dmbpy), 4,4′-di-*tert*-butyl-2,2′-bipyridine (4,4′-dtbbpy), K_2PtCl_4, and K_2PdCl_4 were purchased from Aldrich. $IrCl_3 \cdot 4H_2O$ was purchased from Pressure Chemical Company. Triethanolamine (TEOA) and triethylamine (TEA) were purchased from Alfa Aesar. Acetonitrile (ACN), N,N′-dimethylformamide (DMF), and tetrahydrofuran (THF) were purchased from Acros. THF used for photoreactions was distilled over sodium and benzophenone before use, and other commercial materials were used as received.

5-Methyl-2-(4-methoxyphenyl)pyridine (MeO-mppy) and 5-methyl-2-(4-fluorophenyl)pyridine (F-mppy) were synthesized by a Kröhnke pyridine synthesis according to literature procedures.[25,26] The ligands 5,5′-ditetrafluoromethyl-2,2′-bipyridine (dCF_3bpy) and 5,5′-ditrifluoromethyl-2,2′-bipyridine (dFbpy) were synthesized through a nickel-catalyzed homocoupling, as described in the literature.[27,28] The ligand 5,5′-di-*iso*-propyl-2,2′-bipyridine (5,5′-dipbpy) was prepared by treating 5,5′-dmbpy with lithium diisopropylamide along with iodomethane as described in the Supporting Information.

Tetrakis-(C^N)-μ-(dichloro)diiridium(III) complexes were prepared and cleaved to form the desired complexes as previously described.[12,25,29] The compound $[Ir(F\text{-}mppy)_2(dFbpy)](PF_6)$ was synthesized by cleaving the dimer in ACN at 75 °C to avoid the decomposition of dFbpy that was observed at higher temperatures in ethylene glycol. All monomeric iridium complexes were purified through acetonitrile/ether vapor diffusion and characterized by ^1H and ^{13}C NMR on a Bruker BioSpin Advance-500 MHz spectrometer at room temperature (see the Supporting Information for chemical shifts of previously unreported compounds).

Hydrogen Evolution Experiments. The procedure for hydrogen evolution experiments was adapted from a previously described protocol.[21] Samples for photoinduced hydrogen production were prepared in precleaned 40 mL screw-cap glass vials (VWR). Samples were prepared by adding to the vial a 10 mL volume of a 0.5 M SR, 4:1 solvent/H_2O (solvent = ACN, DMF, or THF) solution containing the specified molar quantity of PS. The palladium or platinum catalyst was then added to the system through the addition of a 50 μL volume of aqueous

(24) Lowry, M. S.; Bernhard, S. *Chem.—Eur. J.* **2006**, *12*, 7970–7977.
(25) Lowry, M. S.; Hudson, W. R.; Pascal, R. A.; Bernhard, S. *J. Am. Chem. Soc.* **2004**, *126*, 14129–14135.
(26) Lowry, M. S.; Goldsmith, J. I.; Slinker, J. D.; Rohl, R.; Pascal, R. A.; Malliaras, G. G.; Bernhard, S. *Chem. Mater.* **2005**, *17*, 5712–5719.
(27) Chan, K. S.; Tse, A. K. S. *Synth. Commun.* **1993**, *23*, 1929–1934.
(28) Fukuda, Y.; Seto, S.; Furuta, H.; Ebisu, H.; Oomori, Y.; Terashima, S. *J. Med. Chem.* **2001**, *44*, 1396–1406.
(29) Sprouse, S.; King, K. A.; Spellane, P. J.; Watts, R. J. *J. Am. Chem. Soc.* **1984**, *106*, 6647–6653.

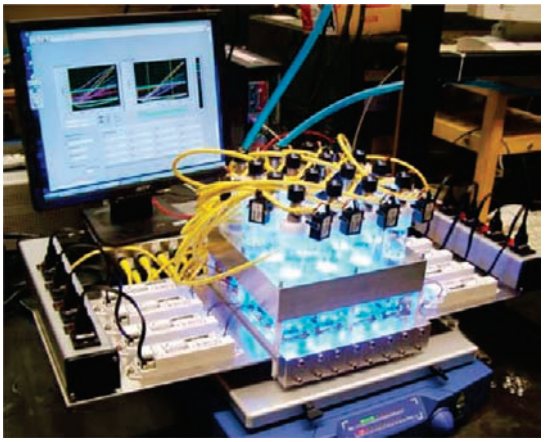

Figure 2. Sixteen-well LED photoreactor equipped with pressure transducers for time-resolved parallel sample analysis. The power output of the LEDs into each sample is 500 ± 50 mW, and the entire array is mounted on a water-cooled aluminum block that is placed on an orbital shaker.

6 mM K_2PdCl_4 or K_2PtCl_4 (300 nmol). Sample vials were deoxygenated by undergoing 10 iterations of an applied low vacuum for a period of 60 s and followed by an overpressure of argon. The vial headspace pressure was brought to atmospheric pressure after the final iteration. The vials were then placed in a home-built 16-compartment sample holder and illuminated from below, as shown in Figure 2. The light-emitting diodes (LEDs) have a peak wavelength of 460 nm with a 20 nm full-width at half-maximum (Luxeon V Dental Blue, Future Electronics) and were equipped with collimating optics (Fraen, FHS-HNB1-LL01-H) to give a total output power of 500 ± 50 mW. The LEDs were driven at 700 mA using a Xitanium Driver (Advance Transformer Company) and were fixed to a copper plate situated on a water-cooled aluminum block. The entire setup was agitated at 150 rpm using an orbital shaker (IKA, KS 260). Hydrogen evolution was monitored through the use of temperature-compensating pressure transducers (Omega PX-138-030A5 V). The transducers were driven in parallel at 8 V using a variable-power supply (Temna 72−2005). Pressure readings were corrected by referencing the pressure of sample vials to the pressure of a vial containing a 10 mL volume of 0.5 M SR in 4:1 solvent/H_2O. After gas evolution had ceased, vials maintained a static pressure for several hours in all cases. This confirmed the absence of leaks or back reactions that consumed hydrogen gas. The output from the pressure transducers was scaled by analyzing the reaction's headspace with a residual gas analyzer (Standard Research System QMS Series Gas Analyzer) that was calibrated using reference standards of 1:9 H_2/Ar and 1:1 H_2/Ar (Airgas). Unless otherwise specified, studies were conducted at room temperature. For varied-temperature studies, the samples were deoxygenated at room temperature and then placed into a 5-cm-thick aluminum block connected to a recalculating chiller at the specified temperature (VWR 1173MD). The samples were allowed to thermally equilibrate for 10−15 min, while the temperature of a reference sample was monitored using a thermocouple (VWR 77776-726). When a static pressure and temperature was reached, the samples were illuminated and analyzed as previously described.

Hydrogen production was calculated according to the ideal gas law assuming 1 atm, 298 K, and a combined vial and transducer adapter headspace that was measured to be 34.5 mL. PS turnover numbers (TONs) refer to the total number of one-electron proton reductions achieved by the time hydrogen evolution had ceased divided by the quantity of PS contained in the initial reaction mixture. Maximum turnover frequency (TOF) reflects the maximum number of PS turnovers per time as recorded by hydrogen evolution rate data. The quantum yield of dihydrogen production (Φ_{H_2}) was calculated by dividing the TOF by the absorbed photon flow that was determined from the PS molar absorptivity using a 2 cm path length, the LED's 500 mW power, and an average wavelength of 460 nm.

Metal Catalyst Stability Experiments. The in situ palladium or platinum catalyst stability of different reaction mixtures was tested through a series of injections. Two identical samples of each type of reaction mixture (PS = 10 μmol $[Ir(ppy)_2(bpy)](PF_6)$, catalyst = K_2PdCl_4 or K_2PtCl_4, SR = TEA or TEOA, solvent = ACN) were prepared, deoxygenated, and illuminated according to the protocol described previously. For each reaction mixture, one of the prepared samples was a test vial used to assess the catalyst stability. The other sample served as a control. After hydrogen evolution was observed to be very slow or stopped (after approximately 6 h of illumination), an injection containing 1.0 mL of a 10 mM photosensitizer, 4:1 ACN/H_2O solution was injected through a rubber septum into the test vial with a syringe. Immediately afterward, an injection containing 1.0 mL of a 4:1 ACN/H_2O solution was similarly injected into the control. The solutions injected into the vials had been degassed by bubbling with ACN-saturated nitrogen for a period of 15 min prior to injection. Samples were further illuminated until hydrogen production reached a second plateau. An example of a raw kinetic trace from one such experiment is included in the Supporting Information.

Transmission Electron Microscopy Measurements. Transmission electron microscopy was performed on a Ziess 910 TEM using an accelerating voltage of 100 keV. Samples were prepared by evaporating the hydrogen-producing solution on a holey carbon-coated copper grid (SPI supplies). Sample size analysis was performed using 100 particles.

Catalyst Poisoning Experiments. Three vials containing 10 mL of 100 μM $[Ir(ppy)_2(bpy)](PF_6)$, 30 μM K_2PdCl_4, and 0.5 M TEA in 4:1 THF/H_2O were prepared. The solutions were then deoxygenated, illuminated for a period of 2.6 h, and analyzed as described above. After residual gas analysis, 500 equiv of Hg(0) per initial amount of Pd was added to one of the vials, and 2500 equiv of Hg(0) was added to one of the other vials. The third vial was kept as a control and not exposed to Hg(0). The samples were then stirred in the dark for 0.8 hours. All three vials were then deoxygenated as described above, subjected to a second period of illumination, and analyzed according to procedure. The experimental protocols for additional Hg(0) poisoning control experiments and their results can be found in the Supporting Information.

Photophysical and Electrochemical Measurements. For photophysical measurements, solutions were made using a solvent of 4:1 ACN/H_2O unless stated otherwise. UV−vis spectra of 300 μM PS solutions were recorded at room temperature in a 1.0 cm quartz cuvette using a Hewlett-Packard 8453 spectrometer equipped with a diode-array detector. Photoluminescences of 30 μM PS solutions were recorded by using a Jobin-Yvon Fluorolog-3 spectrometer equipped with double monochromators and a Hamamatsu-928 photomultiplier tube (PMT) as the detector at right-angle geometry. Solutions were deoxygenated by bubbling with ACN-saturated nitrogen gas for a period of 20 min. Samples were excited at 400 nm, and all emission spectra were adjusted according to the calibrated correction factors for the instrument. Spectra were collected in the range of 420−700 nm, with data points every 2 nm. Excited-state lifetimes (τ) of 30 μM PS solutions were measured using the emission monochromators and the PMT detector of the Jobin-Yvon Fluorolog-3 spectrometer. The samples were excited at 337 nm with a N_2 laser (Laser Science, Inc. VSL-337LRF, 10 ns pulse), and the emission decay was recorded using a Tektronix TDS 3032B digital phosphor oscilloscope. Quenching constants (k_q) were determined by measuring excited state lifetimes at multiple SR concentrations (up to 1.0 M) in a 30 μM PS 4:1 ACN/H_2O solution and applying a Stern−Volmer analysis.

Emission quantum yields (Φ_{em}) were calculated relative to a 30 μM $[Ru(bpy)_3](PF_6)_2$ in ACN reference ($\Phi_r = 0.062$),[30] as described previously.[25] For measurements at varied temperatures, a heat bath was used to circulate water through the sample chamber. At the beginning of the studies, solutions were degassed by bubbling with ACN-saturated nitrogen for 20 min. Between measurements, samples were degassed by bubbling with ACN-saturated nitrogen for 5 min before being thermally equilibrated in the sample chamber for 5 min. Emission and lifetime measurements were conducted as described above using PS solutions in ACN, and the resulting rates of all nonradiative (k_{nr}) and radiative (k_r) proceses were determined according to eqs 1 and 2 below.[31]

$$k_{nr} = \frac{(1-\Phi_{em})}{\tau} \quad (1)$$

$$k_r = \tau^{-1} - k_{nr} \quad (2)$$

Cyclic voltammetry was carried out at 100 mV/s in 5.0 mL of 0.5 mM PS, 0.1 M tetrabutylammonium hexafluorophosphate in ACN with a 1 mm^2 platinum working electrode, a platinum counter electrode, and a silver wire as a pseudoreference. The solution was deoxygenated for a period of 20 min by bubbling it with nitrogen. Data were referenced using the ferrocene oxidation potential (0.371 V vs saturated calomel electrode) as an internal standard.

Results and Discussion

Metal Catalyst and Sacrificial Reductant Comparison. Different sacrificial reductants (TEOA, TEA) and metal catalysts (K_2PtCl_4, K_2PdCl_4) were initially tested to investigate the effects of the SR and metal catalyst on hydrogen evolution (10 mL of 1 mM $[Ir(ppy)_2(bpy)](PF_6)$, 30 μM catalyst, 0.5 M SR in 4:1 ACN/H_2O). K_2PtCl_4 and K_2PdCl_4 were added as salts. While previous data suggest that the catalyst's active form is colloidal,[21] the method of introducing the catalyst as the salt precursor was found to be the most reproducible. Kinetic traces of hydrogen evolution over the course of illumination for each system can be seen in Figure 3. Initial hydrogen evolution rates depended primarily on the choice of metal catalyst, with K_2PtCl_4 allowing for faster initial catalytic rates. Despite the difference in quenching kinetics between TEA ($k_q = 1.9 \times 10^7\ M^{-1}\ s^{-1}$) and TEOA ($k_q = 6.4 \times 10^6\ M^{-1}\ s^{-1}$), the choice of SR did not have a systematic effect on initial rates. However, the TEA systems did exhibit longer-lived catalysis, as evidenced by the slower decay of their initial hydrogen evolution rates.

To evaluate the stability of the metal catalyst over the course of illumination, a series of tests was conducted in which an additional 10 μmol of $[Ir(ppy)_2(bpy)](PF_6)$ in a 1 mL solution of 4:1 ACN/H_2O was injected into each of the four different systems (SR = TEA, TEOA; catalyst = K_2PtCl_4, K_2PdCl_4) after the systems' activities had slowed substantially. By replacing the degraded photosensitizer with these injections, this study allowed for an assessment of the state of the Pd or Pt catalyst after the first phase of illumination. Kinetic traces for the initial

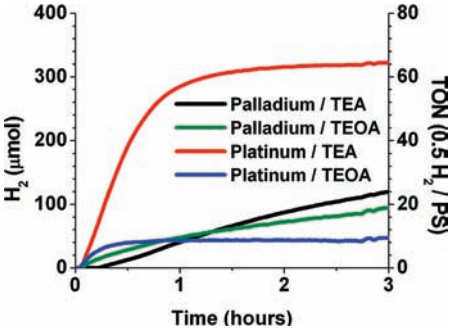

Figure 3. Kinetic traces of the initial hydrogen evolution in systems utilizing different metal catalysts (K_2PdCl_4, K_2PtCl_4) and SR (TEA, TEOA). Reaction mixtures contained 10 mL of 1 mM $[Ir(ppy)_2(bpy)](PF_6)$, 30 μM metal catalyst, and 0.5 M SR in 4:1 ACN/H_2O.

hydrogen production (black) and hydrogen production after the 1 mL addition of PS solution after 6 h of illumination (red) can be seen in Figure 4. Renewed hydrogen evolution after PS addition shows the enhanced robustness of the palladium catalyst (Figure 4A,B) compared to the platinum catalyst (Figure 4C,D). The accelerated kinetics of the palladium systems upon a second PS addition suggests that the catalytic activity of the palladium colloid that is formed in situ continues to increase for the first several hours of the reaction, while the active platinum catalyst presumably forms and decomposes on a much shorter time scale. In a series of control experiments, when reaction vials with the four different initial compositions were injected with a PS-deficient 1 mL mixture of 4:1 ACN/H_2O after 6 h of illumination, only negligible hydrogen evolution was observed in the post-injection time period. These studies help to illustrate the trade-off between catalyst activity and stability. The consistency of the palladium/TEA system allows for the observation of PS structure effects on hydrogen evolution with limited convolution from Pd catalyst decomposition and is used in subsequent studies for the evaluation of PS performance.

Photosensitizer Studies: Steric and Electronic Considerations. To investigate the impact of synthetic modification on PS performance, a combinatorial library using three C^N ligands and five N^N ligands was synthesized. The chemical structures and net turnover data from these PSs in the robust palladium/TEA system (10 mL of 1 mM PS, 30 μM K_2PdCl_4, and 0.5 M TEA in 4:1 ACN/H_2O) are shown in Figure 5. Structural modification dramatically affects PS performance, and 13 of the tested PSs exhibited higher turnover numbers than that of the standard $[Ir(ppy)_2(bpy)]^+$ structure. The most active catalytic system, which employed the $[Ir(MeO\text{-}mppy)_2(5,5'\text{-}dipbpy)]^+$ PS, produced almost 6 times the total amount of hydrogen evolved with $[Ir(ppy)_2(bpy)]^+$.

While the series of $[Ir(MeO\text{-}mppy)_2(N^\wedge N)]^+$ and $[Ir(F\text{-}mppy)_2(N^\wedge N)]^+$ complexes systematically produced more hydrogen than $[Ir(ppy)_2(N^\wedge N)]^+$ complexes for a given N^N ligand, this result is not easily attributed to differences in the PS photophysical parameters. As shown in Table 1, $[Ir(F\text{-}mppy)_2(N^\wedge N)]^+$ complexes exhibit longer excited-state lifetimes compared to $[Ir(ppy)_2(N^\wedge N)]^+$ PS structures, whereas $[Ir(MeO\text{-}mppy)_2(N^\wedge N)]^+$ complexes have comparatively short lifetimes.

(30) Caspar, J. V.; Meyer, T. J. *J. Am. Chem. Soc.* **1983**, *105*, 5583–5590.
(31) Kalyanasundaram, K. *Photochemistry of Polypyridine and Porphyrin Complexes*; Academic Press: New York, 1992; pp 172−173.

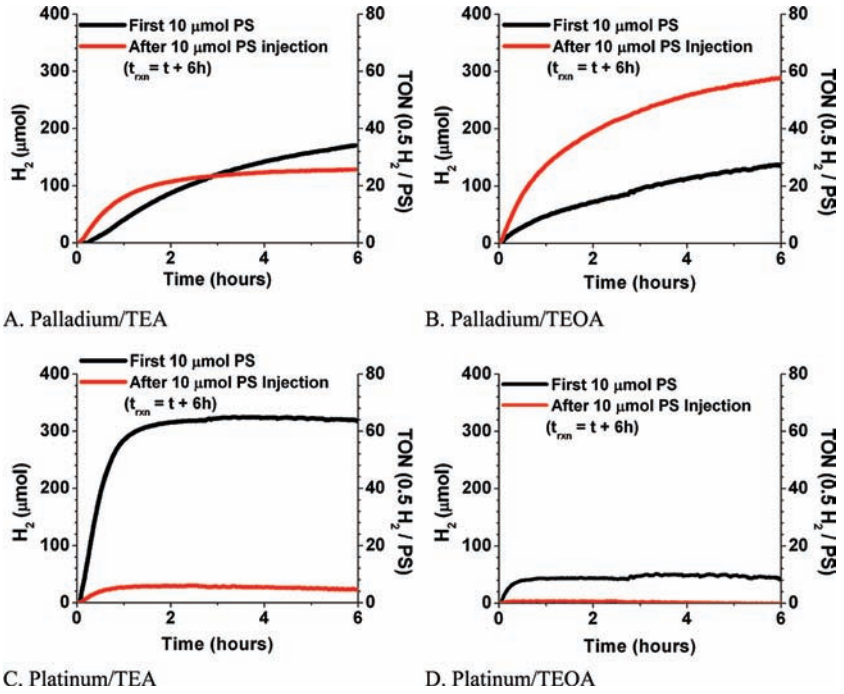

Figure 4. Kinetic traces of hydrogen production of initial reaction mixtures before (black) and after an injection of a second 10 μmol quantity of PS following the initial 6 h illumination period (red). Control vials injected with a PS-deficient solvent produced minimal amounts of H_2 during the second phase of illumination. Initial reaction mixtures consisted of 10 mL of 1 mM $[Ir(ppy)_2(bpy)](PF_6)$, 30 μM metal catalyst, and 0.5 M SR in 4:1 ACN/H_2O. (See the Supporting Information for a graphical description of the experimental protocol.)

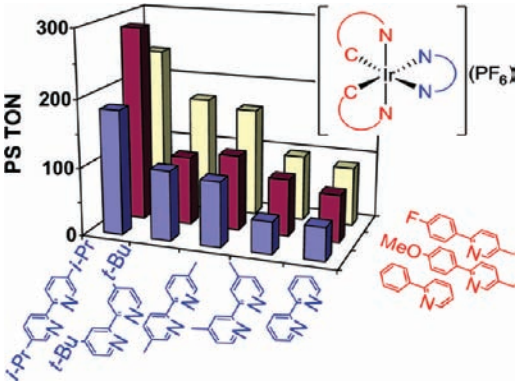

Figure 5. $[Ir(C^{\wedge}N)_2(N^{\wedge}N)](PF_6)$ PS performance in photoreactions. The library outlines structure−activity correlations, and the observed trends show that $N^{\wedge}N$ ligand modification yields a systematic change in catalytic performance independent of the $C^{\wedge}N$ ligand used (and vice versa). Reaction mixtures consisted of 10 mL of 1 mM PS, 30 μM K_2PdCl_4, and 0.5 M TEA in 4:1 ACN/H_2O.

In addition, the $[Ir(F\text{-}mppy)_2(N^{\wedge}N)]^+$ complexes have more positive redox potentials than $[Ir(ppy)_2(bpy)]^+$ analogs, while the $[Ir(MeO\text{-}mppy)_2(N^{\wedge}N)]^+$ complexes have comparatively negative redox potentials (see the Supporting Information). Furthermore, $[Ir(F\text{-}mppy)_2(N^{\wedge}N)]^+$ complexes exhibit the smallest molar extinction coefficients of the investigated photosensitizers, while $[Ir(MeO\text{-}mppy)_2(N^{\wedge}N)]^+$ complexes show absorptivity similar to $[Ir(ppy)_2(N^{\wedge}N)]^+$ species. Lifetime and molar absorptivity have previously been used in an effort to predict efficient PS performance,[12] but they do not appear to determine photosensitizer performance in the catalytic system presented here. With the combinatorial approach, the identification of previously unknown structure−activity trends has been possible. The independent impact of $C^{\wedge}N$ and $N^{\wedge}N$ modification on hydrogen production, as shown by the systematic trends in Figure 5, demonstrates how the heteroleptic ligand architecture can be used to optimize catalytic performance and stability.

One possible explanation for the increased catalytic performance of both $[Ir(F\text{-}mppy)_2(N^{\wedge}N)]^+$ and $[Ir(MeO\text{-}mppy)_2(N^{\wedge}N)]^+$ photosensitizers is the influence of steric bulk on compound stability. As shown in Figure 6, $[Ir(F\text{-}mppy)_2(5,5'\text{-}dipbpy)]^+$ and $[Ir(MeO\text{-}mppy)_2(5,5'\text{-}dipbpy)]^+$ maintain catalytic activity for a greater duration than $[Ir(ppy)_2(5,5'\text{-}dipbpy)]^+$. The impact of steric contributions can also be seen through $N^{\wedge}N$ ligand modification. $[Ir(C^{\wedge}N)_2(4,4'\text{-}dtbbpy)]^+$ outperforms $[Ir(C^{\wedge}N)_2(4,4'\text{-}dmbpy)]^+$ for a given $C^{\wedge}N$ ligand despite exhibiting similar photophysical properties. The increased hydrogen production concurrent with greater steric bulk was also observed for $[Ir(C^{\wedge}N)_2(5,5'\text{-}dipbpy)]^+$ and $[Ir(C^{\wedge}N)_2(5,5'\text{-}dmbpy)]^+$. The use of bulkier ligands minimizes solvent access to the iridium center, which presumably stabilizes the PS by hindering ligand substitution. Correlation of steric shielding with increased hydrogen evolution has also been observed in a previous system utilizing a homogeneous rhodium-based catalyst, where bulkier ligands also serve to enhance PS stability.[22]

As shown above, $N^{\wedge}N$ ligand substituents have a systematic and dramatic impact on PS performance for a constant $C^{\wedge}N$ ligand. To exploit this effect and further probe the observed enhanced activity of complexes of F-mppy, two novel $[Ir(F\text{-}mppy)_2(N^{\wedge}N)]^+$ structures ($N^{\wedge}N$ = dCF_3bpy and dFbpy) were characterized and tested as PSs (10 mL of 1 mM PS, 30 μM K_2PdCl_4, and 0.5 M TEA in 4:1 ACN/H_2O). The time-resolved hydrogen evolution data of the novel structures, along with $[Ir(F\text{-}mppy)_2(bpy)]^+$ for reference and $[Ir(F\text{-}mppy)_2(5,5'\text{-}dmbpy)]^+$ as

Table 1. Photophysical Properties and Hydrogen Production Data of $[Ir(C^{\wedge}N)_2(N^{\wedge}N)](PF_6)$ PS Structures[a]

C^N Ligand	N^N Ligand	E_{em} (eV)	k_{nr} (s^{-1})	τ (ns)	ε (M^{-1} cm^{-1}) at 465 nm	PS TON (0.5 H_2/PS)	max. PS TOF (TON/h)
ppy	bpy	2.11	2.57×10^6	370	597	49	9
ppy	4,4′-dmbpy	2.18	1.63×10^6	549	573	47	67
ppy	4,4′-dtbbpy	2.18	1.33×10^6	651	460	103	120
ppy	5,5′-dmbpy	2.23	5.40×10^5	1271	570	96	95
ppy	5,5′-dipbpy	2.22	5.20×10^5	1346	530	184	104
F-mppy	bpy	2.23	9.31×10^5	869	397	87	45
F-mppy	4,4′-dmbpy	2.28	6.79×10^5	995	294	97	84
F-mppy	4,4′-dtbbpy	2.29	6.08×10^5	1027	329	170	135
F-mppy	5,5′-dmbpy	2.35	2.53×10^5	1475	340	160	162
F-mppy	5,5′-dipbpy	2.33	2.54×10^5	1488	330	239	148
F-mppy	dFbpy	2.24	6.35×10^5	1165	318	312	21
F-mppy	dCF_3bpy	*b*	*b*	*b*	663	99	99
MeO-mppy	bpy	2.10	5.34×10^6	185	623	70	43
MeO-mppy	4,4′-dmbpy	2.15	3.37×10^6	286	470	84	55
MeO-mppy	4,4′-dtbbpy	2.15	2.61×10^6	364	527	101	101
MeO-mppy	5,5′-dmbpy	2.21	9.68×10^5	890	520	111	114
MeO-mppy	5,5′-dipbpy	2.20	1.09×10^6	820	570	288	121

[a] Photophysical measurements conducted in 4:1 ACN/H_2O solutions. Catalytic parameters (TON = turnover numbers achieved by the time hydrogen evolution had stopped; TOF = maximum turnover frequency during photoreaction) reflect the activity of reaction mixtures that consisted of 10 mL of 1 mM PS, 30 μM K_2PdCl_4, and 0.5 M TEA in 4:1 ACN/H_2O. [b] No luminescence observed.

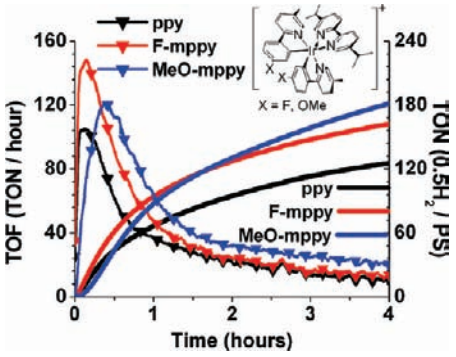

Figure 6. Kinetic traces for PS turnovers (right axis, bold lines) and turnover frequency (left axis, triangular symbols) for $[Ir(C^{\wedge}N)_2(5,5'\text{-dipbpy})](PF_6)$ over the course of illumination. Reaction mixtures consisted of 10 mL of 1 mM PS, 30 μM K_2PdCl_4, and 0.5 M TEA in 4:1 ACN/H_2O.

a control for steric effects, are shown in Figure 7. Photophysical characterization of the novel PS structures can be found in Table 1, and redox potentials are tabulated in Table S1 in the Supporting Information. The inclusion of these new compounds allowed for a more thorough investigation of N^N ligand effects. All bpy ligand derivatives tested in the combinatorial study outlined in Table 1 were substituted with electropositive alkyl groups, and thus the influence of N^N electronic effects could not be tested independently from steric bulk. dCF_3bpy and dFbpy have electronegative substituents that are expected to be sterically similar to the methyl groups in 5,5′-dmbpy and, therefore, allow for a more complete investigation of $[Ir(C^{\wedge}N)_2(N^{\wedge}N)]^+$ ligand effects.

The results from Figure 7 in conjunction with the initial study provide new insight into relationships between a complex's structure and its PS performance. The proposed advantage of steric bulk is confirmed, as $[Ir(\text{F-mppy})_2(X_2\text{-bpy})]^+$ structures with both electronegative and electropositive N^N substituents show increased hydrogen production. The sharp decline in catalytic activity of $[Ir(\text{F-mppy})_2(dCF_3bpy)]^+$ compared to the longer catalytic lifetime observed for other species after an hour of illumination (Figure 7B) suggests that its lower TON can be partially attributed to N^N ligand electronic effects on catalyst stability. The longer induction period and slower reaction kinetics observed for $[Ir(\text{F-mppy})_2(\text{dFbpy})]^+$ suggest that there is a unique interaction between this PS structure and the palladium catalyst. However, the existence of such interactions remains difficult to assess with contemporary techniques due to the inherent reaction complexity.

Solvent Studies. When iridium PS degradation products were previously identified in a water-reducing system utilizing a platinum catalyst, one unambiguously observed decomposition product was $[Ir(ppy)_2(ACN)]^+$.[21] Therefore, solvent is directly involved in PS decomposition in this water-reducing system. To investigate the impact of solvent effects on catalysis, DMF and THF were employed as alternatives to ACN and tested using $[Ir(ppy)_2(bpy)]^+$, $[Ir(\text{F-mppy})_2(bpy)]^+$, and $[Ir(\text{F-mppy})_2(\text{dFbpy})]^+$ as photosensitizers (10 mL of 100 μM PS, 30 μM K_2PdCl_4, and 0.5 M TEA in 4:1 solvent/H_2O). Both THF and DMF showed superior performance compared to ACN, as indicated by the systems' net hydrogen production shown in Figure 8. DMF and THF systems demonstrated both higher catalytic activity and enhanced stability, as shown by the representative kinetics of $[Ir(\text{F-mppy})_2(bpy)]^+$ in Figure 9. The weaker ligand strength of DMF and THF ligands results in slower photodecomposition of the PS, thus explaining the enhanced system stability in these alternative solvents.

As demonstrated in Figure 8, each solvent system investigated preserves the identified trends between PS structures and hydrogen production. This suggests that PS behavior is similar under the different conditions and that solvent choice in this case does not significantly impact the observation of trends in comparative PS studies. However, the significantly higher number of catalytic turnovers achievable using THF allows for the testing of PS capability limits. In addition, higher net hydrogen production allows for reliable gas measurements using small molar quantities of PS salts, thus conserving resources. THF was therefore selected as the

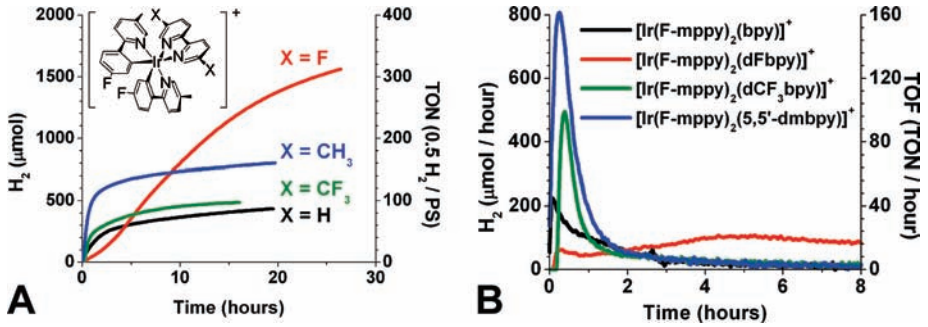

Figure 7. Time-resolved catalytic data for novel $[Ir(F\text{-}mppy)_2(N^{\wedge}N)]^+$ PS structures, $[Ir(F\text{-}mppy)_2(bpy)]^+$, and $[Ir(F\text{-}mppy)_2(5,5'\text{-}dmbpy)]^+$. Cumulative hydrogen production (inset A) and the rate of hydrogen production (inset B) are shown over the course of illumination. Reaction mixtures contained 10 mL of 1 mM PS, 30 μM K_2PdCl_4, and 0.5 M TEA in 4:1 ACN/H_2O.

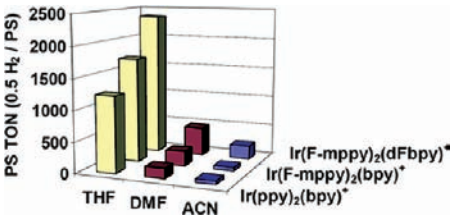

Figure 8. Net hydrogen evolution of selected photosensitizers in various solvents. Reaction mixtures consisted of 10 mL of 100 μM PS, 30 μM K_2PdCl_4, and 0.5 M TEA in 4:1 solvent/H_2O.

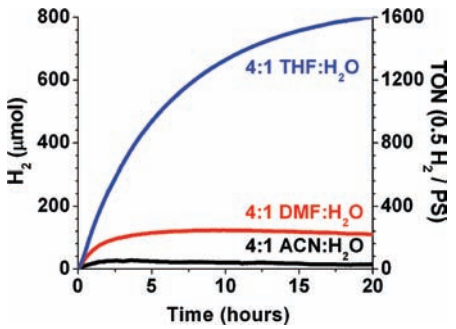

Figure 9. Hydrogen production of $[Ir(F\text{-}mppy)_2(bpy)]^+$ in different solvents over time. Reaction mixtures consisted of 10 mL of 100 μM $[Ir(F\text{-}mppy)_2(bpy)](PF_6)$, 30 μM K_2PdCl_4, and 0.5 M TEA in 4:1 solvent/H_2O.

solvent for subsequent temperature studies as the state of the art water reduction system.

Nature of the Active Catalyst. Previous examples have shown that molecular platinum and palladium species can be reduced to form a colloidal catalyst under similar conditions to those applied in the present study.[15,20,21,32] To ensure that heterogeneous catalysts are forming, TEM analysis was conducted on an aliquot of an active photocatalytic reaction (10 mL of a solution that is 100 μM $[Ir(ppy)_2(bpy)](PF_6)$, 30 μM K_2PdCl_4, and 0.5 M TEA in 4:1 THF/H_2O) both prior to illumination and after 18 min of illumination. The irradiated sample showed the presence of small, electron-dense particles with an average size of 3 ± 1 nm (mean $\pm$ sd), which can be seen in the transmission electron micrograph in Figure 10. These particles were not present prior to illumination, which supports the conclusion that colloid formation occurs during early time points in the photoreaction.

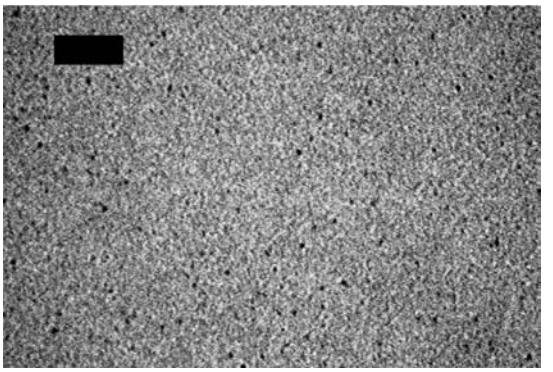

Figure 10. Transmission electron micrograph of an aliquot of a photocatalytic reaction containing 10 mL of 100 μM $[Ir(ppy)_2(bpy)]PF_6$ and 30 μM K_2PdCl_4 in 0.5 M TEA in 4:1 THF/H_2O showing the presence of a small metal colloid in the reaction medium. Sample was taken after 18 min of illumination. Scale bar = 50 nm.

The presence of nanoparticles alone does not confirm the presence of an active colloidal catalyst. To determine that the colloid is the active species, a series of mercury poisoning experiments was conducted. Pd(0) is known to form an amalgam with mercury, and the catalytic system should be deactivated in the presence of mercury if the colloid is indeed the active catalyst.[33] When a quantity of mercury was added and stirred in reaction mixtures after 2.6 h had elapsed, the systems showed either reduced (500 Hg equiv) or no catalytic activity (2500 Hg equiv) during a second phase of illumination, as shown in Figure 11. It is unlikely that the added mercury diminishes system performance by degrading the PS, as the system's activity is not substantially affected when the reaction mixture is pretreated with mercury prior to illumination (see Figure S2 in the Supporting Information). It was demonstrated that vigorous stirring of the reaction mixture was required to form the amalgam, as reaction mixtures containing Hg(0) showed similar catalytic activity to mercury-deficient controls in the absence of stirring (see Figure S3 in the Supporting Information). These tests, along with TEM observation of nanoparticle formation during illumination, demonstrate that a colloidal metal catalyst is indeed the active catalytic species in the system.

Temperature Studies. In order to further probe and understand the kinetic behavior of the catalytic systems, hydrogen evolution of two different photosensitizers with

(32) Lehn, J. M.; Sauvage, J. P. *Nouv. J. Chim.* **1977**, *1*, 449–451.

(33) Widegren, J. A.; Finke, R. G. *J. Mol. Catal. A: Chem.* **2003**, *198*, 317–341.

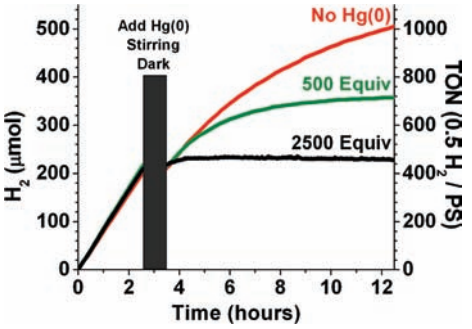

Figure 11. Mercury poisoning experiment supporting the claim that colloidal metal formed in situ is the active catalytic species. Reduced catalytic activity upon additions of 500 (green) and 2500 (black) equivalents of Hg(0) per Pd compared to a Hg(0)-deficient control vial (red) indicates the formation of an amalgam. Initial reaction mixtures consisted of 10 mL of 100 μM $[Ir(ppy)_2(bpy)](PF_6)$, 30 μM K_2PdCl_4, and 0.5 M TEA in 4:1 THF/H_2O.

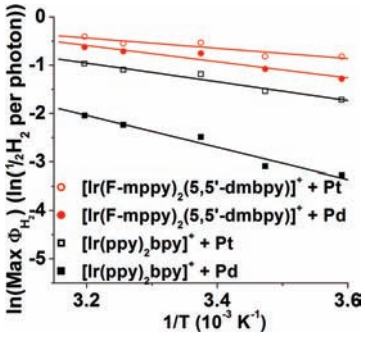

Figure 12. Reaction kinetics for selected photosensitizers at varied temperatures. Arrhenius behavior is observed, and the resulting activation energies ($\Delta G_{exp}^{\ddagger}$) are given in Table 2. Reaction mixtures consisted of 10 mL of 100 μM PS, 30 μM K_2MCl_4 (M = Pt, Pd), and 0.5 M TEA in 4:1 THF/H_2O.

Pt or Pd catalysts was monitored at five different temperatures (10 mL of 100 μM PS, 30 μM K_2PtCl_4 or K_2PdCl_4, and 0.5 M TEA in 4:1 THF/H_2O). The adherence of the data to Arrhenius behavior, as shown in Figure 12, indicates the constancy of the system and the robust nature of the active palladium or platinum catalyst to temperature variations.

Slower reaction kinetics and a higher activation energy of the rate-determining step were observed for palladium compared to those of platinum in the 4:1 THF/H_2O system for both $[Ir(ppy)_2(bpy)]^+$ and $[Ir(F\text{-}mppy)_2(5,5'\text{-}dmbpy)]^+$, which is in agreement with other studies that compare the catalytic efficiencies of Pt and Pd colloids for hydrogen evolution.[34] However, the PS structure also affects the temperature dependence of the catalytic rates, as shown in Table 2, thus indicating that the rate-determining step depends on the PS structure as well as the nature of the metal catalyst. Hydrogen formation in a system utilizing $[Ir(F\text{-}mppy)_2(5,5'\text{-}dmbpy)]^+$ with either the Pt or Pd catalysts shows less of a temperature dependence than $[Ir(ppy)_2(bpy)]^+$ and therefore has a lower activation energy for the rate-determining step. It is believed that the increased electron-transfer driving force of 0.1 V for $[Ir(F\text{-}mppy)_2(5,5'\text{-}dmbpy)]^+$ relative to $[Ir(ppy)_2(bpy)]^+$ from the reduced photosensitizer (PS^-)

(34) Amouyal, E.; Koffi, P. *J. Photochem.* **1985**, *29*, 227–242.

Table 2. Activation Energies ($\Delta G_{exp}^{\ddagger}$) of Photoreactions Consisting of 10 mL of 100 μM PS, 30 μM K_2MCl_4 (M = Pt, Pd), and 0.5 M TEA in 4:1 THF/H_2O[a]

PS	catalyst	$\Delta G_{exp}^{\ddagger}$
$[Ir(ppy)_2(bpy)]^+$	Pd	27 kJ/mol
$[Ir(ppy)_2(bpy)]^+$	Pt	16 kJ/mol
$[Ir(F\text{-}mppy)_2(5,5'\text{-}dmbpy)]^+$	Pd	14 kJ/mol
$[Ir(F\text{-}mppy)_2(5,5'\text{-}dmbpy)]^+$	Pt	8.8 kJ/mol

[a] The observed activation energies are dependent on both the nature of the catalyst and the choice of photosensitizer.

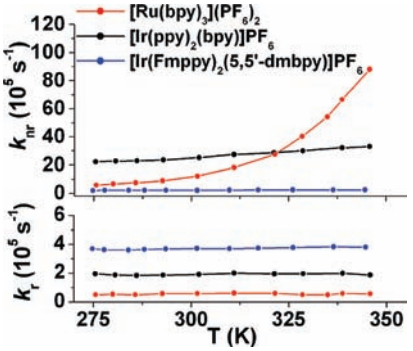

Figure 13. Temperature dependence of nonradiative decay (k_{nr}) and radiative decay (k_r) of $[Ru(bpy)_3](PF_6)_2$, $[Ir(ppy)_2(bpy)]PF_6$, and $[Ir(F\text{-}mppy)_2(5,5'\text{-}dmbpy)]PF_6$ in ACN. Temperature independence of nonradiative decay is expected for the iridium(III) complexes to be due to thermal inaccessibility of the MC state.

to the metal colloid is responsible for the lower activation energy when either a Pt or Pd catalyst is employed (see Table S1 in the Supporting Information).

To ensure that the observed temperature dependence on the photocatalytic rate was not convoluted by the altered photophysical properties of the PSs at varied temperatures, the rates of nonradiative and radiative decay of several PSs were examined as a function of the temperature. While an increase in temperature is known to decrease the excited-state lifetimes of Ru(II) complexes exhibiting similar metal-to-ligand charge-transfer-based emission,[35−38] the iridium(III) photosensitizers do not demonstrate a significant excited-state lifetime variation in the temperature region explored, as shown in Figure 13. The quickly relaxing metal-centered (MC) state of the iridium-based photosensitizers is not thermally populated in this temperature range, and therefore there is a negligible temperature dependence on the rates of nonradiative decay for the iridium(III) complexes. On the contrary, the rate of nonradiative decay from the excited state of $[Ru(bpy)_3]^{2+}$ shows an exponential dependence on temperature, which dramatically reduces the excited state lifetime at increased temperatures. This indicates the thermal accessibility of the metal−ligand antibonding MC state and further supports the choice of iridium(III) photosensitizers as more robust replacements for ruthenium(II) PSs.

(35) Barigelletti, F.; Juris, A.; Balzani, V.; Belser, P.; von Zelewsky, A. *J. Phys. Chem.* **1986**, *90*, 5190–5193.
(36) Barigelletti, F.; Juris, A.; Balzani, V.; Belser, P.; von Zelewsky, A. *J. Phys. Chem.* **1987**, *91*, 1095–1098.
(37) Durham, B.; Caspar, J. V.; Nagle, J. K.; Meyer, T. J. *J. Am. Chem. Soc.* **1982**, *104*, 4803–4810.
(38) van Houten, J.; Watts, R. J. *J. Am. Chem. Soc.* **1976**, *98*, 4853–4858.

Conclusion

We have reported an electron-relay-deficient catalytic water-reducing system utilizing a palladium catalyst that is capable of probing photosensitizer performance more directly than previously described systems. Through the investigation of a combinatorial library of heteroleptic Ir(III) photosensitizers, we have identified the benefits of designing steric bulk and electropositive N^N ligand substituents into PS structures. This investigation demonstrates the merit of applying a high-throughput approach to the study a complex system like this, as this technique has allowed for the elucidation of previously unknown, systematic structure−activity relationships. Additionally, two novel photosensitizer structures were tested, with $[Ir(F\text{-}mppy)_2(dFbpy)]^+$ achieving greater than 6 times the turnover numbers of the parent $[Ir(ppy)_2(bpy)]^+$ compound under identical conditions. The benefits of weakly ligating solvents were demonstrated, with PS structures achieving turnover numbers in a THF-based solvent that were approximately 10 times those observed in the ACN systems. Through a combination of TEM and mercury poisoning tests, it was shown that the metal catalyst forms an active colloidal species in situ. Temperature studies provided insight into the reaction kinetics, and the resulting Arrhenius behavior allowed for an estimation of the activation energy of the rate-determining step. The resulting activation energies are dependent on both PS structure and the metal catalyst, with the activation energy decreasing with the increased reducing power of reductively quenched PS (PS^-). The insights gained from the systematic variation of PS structure, as well as the probing of the rate-limiting step, allows for an increased understanding of the catalytic process and facilitates the further development of catalytic water reduction systems that could be ultimately coupled with catalytic water oxidation.

Acknowledgment. We thank Neal McDaniel for several useful discussions. S.B. acknowledges support through a NSF CAREER award (CHE-0449755).

Note Added after ASAP Publication. This article was released ASAP on July 16, 2009 with a figure missing from the Supporting Information. The correct version of the Supporting Information was posted on July 20, 2009.

Supporting Information Available: Graphical example of an experiment for screening in situ catalyst stability, from the Pd/TEA system. Electrochemical measurements for selected $[Ir(C^N)_2(N^N)](PF_6)$ photosensitizers. Experimental data for mercury tests and graphs of mercury test control experiments. Synthesis and NMR characterization of 5,5′-dipbpy and NMR characterization of previously unreported iridium complexes. This material is available free of charge via the Internet at http://pubs.acs.org.